INTERMEDIATE TEMPERATURE CERAMIC HEAT PIPE MODELING AND OPTIMIZATION

Andrew van Paridon[1], Giancarlo D'Orazio[1], William R. Sixel[2], and Sadaf Sobhani[1]

[1]Sibley School of Mechanical and Aerospace Engineering, Cornell University, Ithaca, NY 14853, USA
[2]NASA Glenn Research Center, Cleveland, OH, 44135, USA

ABSTRACT

Spacecraft nuclear electric propulsion, as well as other emerging technologies, can benefit from heat pipes with optimal performance in the intermediate temperature, 450–700 K, regime. In this work, a 1D model was developed to investigate the performance of halide working fluids coupled with 3D printed-ceramic shells to operate at 500–600 K and interface with a nuclear electric propulsion system. An initial conceptual design and performance limits of a 3D printed-AlN heat pipe radiator with $AlBr_3$ as the working fluid is presented. An areal density of 5.2kg/m^2 and mass per unit heat performance of 1.00kg/kW is estimated.

I INTRODUCTION

Nuclear Electric Propulsion (NEP) systems are currently the focus of technological maturation as they provide a potential method to support interplanetary missions [1,2]. However, as with all nuclear reactors in space, it is necessary to accommodate the substantial waste heat generated through vast radiators. NASA's Space Technology Mission Directorate (STMD) has identified advancement of radiators as a key technology strategy [3], and set a goal of $\leq$ 3 kg/m^2 areal density and $<$1 kg/kW of mass per unit of heat refection. In a case study for a 2 MW_e reactor conducted by Machemer et al. [4] a 4030 m^2 radiator system is proposed, and such large systems appear to be unavoidable. These radiators could strain the mass budget of spacecraft's overall design. Furthermore, as they need to operate in the temperature range of 500–600 K, there is a reduced field of potential working fluids that could actually facilitate the embedded heat pipes needed to disperse the heat [5]. The intermediate temperature regime of heat pipes, 450–700 K, has not been well characterized due in part to the corrosive nature of many of the working fluids, as well as the poor performance in many conventional metal envelope systems.

Ceramic heat pipes enable broader compatibility with working fluids suitable in the intermediate temperature regime, including halides. In this work, we develop and apply a 1D model to evaluate the areal density of ceramic HPs operating with halide working fluids. The heatflow through a full scale radiator with realistic limits imposed by HP performance is simulated (see Figure 1). Leveraging the potential of ceramic additive manufacturing (AM) for complex structure fabrication [6], we further explore the performance of grooved wicks with a mesh screen liner.

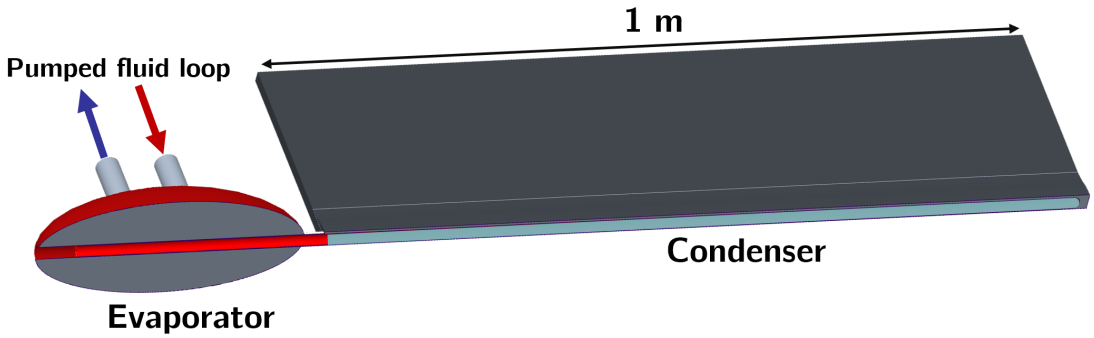

Figure 1: Half-section view of a radiator and heat pipe assembly with pumped fluid loop. The 1D model assumes symmetric radiator panels either side of the heat pipe, and single-sided radiation.

II MATERIAL PROPERTIES

The state-of-the-art combination for shell material and working fluid for HPs at ≈500K is Titanium-Water (Ti-H_2O). Above this temperature water's efficacy drops off quickly. There is also much interest in the commercial heat transfer fluid Dowtherm A (a proprietary blend of diphenyl oxide and biphenyl) to operate in this temperature range. A selection of thermal properties of shell materials and working fluids are shown in Tables 1 and 2 respectively.

Aluminum nitride (AlN) has excellent thermal properties with relatively high thermal conductivity (>120 W/m·K), low bulk density, and high thermal shock resistance. It also has proven to be compatible with a number of working fluids from the halide group [7]. In particular, we will explore the performance when coupled with aluminum bromide ($AlBr_3$). Many halides do not have robust literature regarding their thermal properties, and so a review is underway to compile a baseline framework. This includes potential working fluids of interest such as aluminum chloride ($AlCl_3$), ferric chloride ($FeCl_3$) and antimony bromide ($SbBr_3$).

Typically, ρ is density (kg/m^3), k is thermal conductivity (W/m·K), μ is viscosity (Pa·s)[1], and σ (N/m) is surface tension (σ_y is yield strength in Table 1 only). Furthermore, c_p is specific heat capacity, h_{fg} is enthalpy of vaporization and P_v is vapor pressure. The temperatures $T_{m/b/c}$ represent melting, boiling, and critical temperatures respectively.

[1] 1Pa·s=1000cP

Table 1: Thermodynamic Properties of Shell Material.

Material	Formula	Process	T_m K	ρ kg/m^3	c_p J/kg·K	k_l W/m·K	σ_y MPa
Aluminum Nitride	AlN	Printed	2473*	3255	734	80-120*	300-500*
Titanium (C.P.)	Ti	Milled	1941	4510	528	21	240

*Estimated

Table 2: Thermodynamic Properties of Working Fluid

Fluid	T_m	T_b K	T_c	h_{fg} kJ/kg	P_v MPa	ρ_l kg/m^3	μ_l cP	μ_v cP	k_l W/m·K	σ N/m
$AlBr_3$	371	528	763	172	0.177	2111	0.609	0.0205	0.0879	0.0107
H_2O	273	373	647	1376	6.13	755	0.097	0.019	0.580	0.0197
Dowtherm A	—	530	770	286	0.169	831	0.27	0.01	0.0976	0.0162

$\mapsto$ Evaluated at @$T_{ref} = 550$K as required.

III REDUCED ORDER HEAT PIPE MODEL

III.A Overview

Heat pipes in space work by accumulating heat at the evaporator end and dispersing it along the condenser to the attached radiator fins. Within the HP, the working fluid flows end-to-end and back again, driven by pressure in the evaporator. The pressure is created by surface tension at the fluid-vapor boundary and increases as heat is applied. Performance is limited by a number of mechanisms that restrict this flow, and modelling the performance limits is a useful tool for quickly iterating on design parameters [8], especially when creating accurate conjugate CFD can often be of similar effort to prototyping and testing. A full discussion of HP performance limits is available from Faghri [9].

This model also predicts the heat radiated by two fins that are in direct contact with the condenser length of an isothermal HP, as well as the heat radiated from the HP surface itself. The full description of the 1D radiator model is below. The HP performance limit is calculated for each design iteration, such that an envelope of all limiting mechanisms can be evaluated. Initially, the model assumes a grooved wick, but later a mesh screen liner is added. The HP geometry is shown in Figure 2 and Table 3. Radiator geometry is shown in Figure 3.

Table 3: Input Variables for Heat Pipe and Radiator Geometry.

Lengths		*Radii*		*Grooves*		*Radiator*	
l_e	Evaporator Length	r_o	Outer Radius	w	Channel Width	W	Radiator Width (l_c)
l_a	Adiabatic Length	r_s	Shell Radius	t	Fin Thickness	L	Radiator Length
l_c	Condenser Length	r_i	Inner Radius	d	Depth ($r_s - r_i$)	h	Radiator Thickness

Calculated variables based on geometry include cross sectional areas, surface areas, and volumes. End caps are assumed to be hemispherical for the purposes of completing the

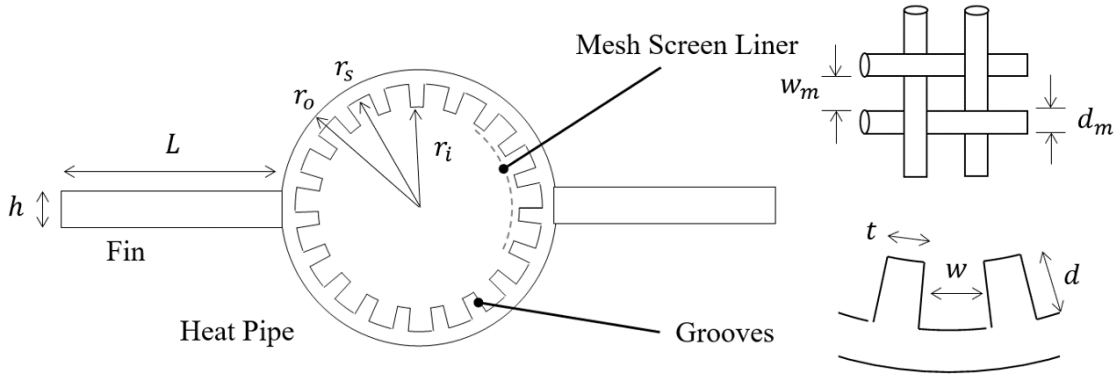

Figure 2: Geometry of Heat Pipe, Radiator and Mesh Screen Liner.

volume calculation. The HP total length l_t and effective length l_{eff} can be defined;

$$l_t = l_e + l_a + l_c \tag{1}$$

$$l_{eff} = (l_e + l_c)/2 + l_a \tag{2}$$

III.B Calculated Parameters

The liquid void fraction ψ can be calculated as the relative fraction of the wick's profile that is filled with fluid under regular operating conditions. This is also known as porosity and Table 4 shows relevant equations. When ψ and volumes are combined with the ρ of the AlN and $AlBr_3$, we can calculate the mass fraction of each component and total mass of a combined HP and radiator.

Another important parameter that varies with wick style is the hydraulic diameter D_h (m). With ψ and D_h we can define the most important properties for assessing HPs, and for which we need to perform trade studies;

- Effective Pore Radius r_{eff} (m) - a measure of the surface area delineating the fluid and vapor regimes at the evaporator, which sets the available pressure head due to the surface tension.

- Permeability K (m^2) - the inverse of resistance when considering the ability of the fluid to transverse from the condenser to the evaporator.

- Effective Thermal Conductivity k_{eff} (W/m·K)- which is found combining the thermal conductivities of the solid k_s and fluid k_f and the wick geometry. *It is not* the same as the conductance implied by the evaporative performance of the HP as a whole.

Typically, the pore radius and permeability are at odds, as the more open (i.e. permeable) a wick design, the greater the surface area at the fluid-vapor interface and thus a lower available pressure [9].

Table 4: Key Parameters for Heat Pipe Performance [9].

Wick Style	ψ (-)	D_h (m)	r_{eff} (m)	K (m^2)	k_{eff} (W/m·K)
Grooved	$\frac{w}{(t+w)}$	$\frac{dw}{2(d+w)}$	w	$\frac{D_h^2\psi}{2(f\,Re_{l,h})}$	$k_s(1-\psi(1-\frac{k_f}{k_s}))$
Sintered*	ψ	$\frac{D\psi}{1-\psi}$	$0.21D$	$\frac{D^2\psi^3}{150(1-\psi^2)}$	$k_s\frac{2+k_f/k_s-2\psi(1-k_f/k_s)}{2+k_f/k_s-\psi(1-k_f/k_s)}$
Mesh Screen†	$1-\frac{1.05\pi N d_m}{4}$	$\frac{d_m\psi}{1-\psi}$	$\frac{w_m+d_m}{2}$	$\frac{D^2\psi^3}{122(1-\psi^2)}$	$k_f\frac{k_f+k_s-(1-\psi)(k_f-k_s)}{k_f+k_s+(1-\psi)(k_f-k_s)}$

*D-Powder Sphere Diameter † N-Mesh Number

III.C Performance Limits

Performance limit formulas can be found in work by Faghri [9]. In the present study, performance is dominated by the *capillary limit*. For a given temperature, the wick can transport a maximum mass flow rate based on capillary action. The product of this maximum mass flow rate and the enthalpy of vaporization is the capillary heat load limit;

$$\dot{Q}_c = \frac{\rho_l \sigma h_{fg}}{\mu_l}\frac{KA_w}{l_{eff}}\left(\frac{2}{r_{eff}} - \frac{\rho_l g l_t}{\sigma}\cos(\theta)\right) \tag{3}$$

where the last term (including gravity g (m/s^2)) represents the gravitational pressure working against a HP inclined at an angle θ. This term is not significant in horizontal HPs nor in space applications. Embedded at the start of this equation is the working fluid merit number M;

$$M = \frac{\rho_l \sigma h_{fg}}{\mu_l} \tag{4}$$

This is often used to compare potential working fluids. It contrasts their ability to carry heat ($\rho_l h_{fg}$) and exert pressure on the vapor (σ), with their resistance to traverse the wick (μ_l). Other limits considered in this work are the;

$$\text{Boiling limit} \quad \dot{Q}_b = \frac{4\pi(l_e)k_{eff}\sigma T_v}{h_{fg}\rho_l \ln(r_s/r_i)}\left(\frac{1}{r_n} - \frac{1}{r_{eff}}\right) \tag{5}$$

$$\text{Viscous limit} \quad \dot{Q}_v = \frac{\pi r_i^4 h_{fg}\rho_v P_v}{12\mu_L l_{eff}} \tag{6}$$

$$\text{Sonic limit} \quad \dot{Q}_s = 0.474 A_v h_{fg}\left(\rho_v P_v\right)^{0.5} \tag{7}$$

$$\text{Entrainment limit} \quad \dot{Q}_e = A_v h_{fg}\left(\frac{\rho_v \sigma}{2r_{cav}}\right)^{0.5} \tag{8}$$

For instance, the *boiling limit* occurs when high heat flux at the evaporator leads to bubble nucleation within the wick structure (rather than at the vapor core boundary) which

inhibits the full flow and wetting of the evaporator end. The *entrainment limit* is an example of a limit that can impede HP efficacy, without necessarily halting the process entirely. This occurs when the speed of the vapor flow creates significant shear stress at at vapor-fluid boundary along the length of the HP. The performance envelope $\dot{Q}_{env}(T)$ is evaluated as the minimum values of the above for the range of temperature under consideration.

III.D Radiator model

The 1D radiator model was designed and validated against that laid out by Juhasz [10]. The temperature profile T of a rectangular fin is evaluated along the x axis, where the fin has divisions Δx with thickness h and width W. Each element has a corresponding surface area dA_s and emissivity ϵ. The temperature at the root of the fin is $T_R = T(0)$ and the far field sink temperature is T_S. The energy balance of each element includes the heat conducted in $\dot{Q}_x$, heat conducted out $\dot{Q}_{x+\Delta x}$ and heat radiated out $\dot{Q}_{rad,x}$.

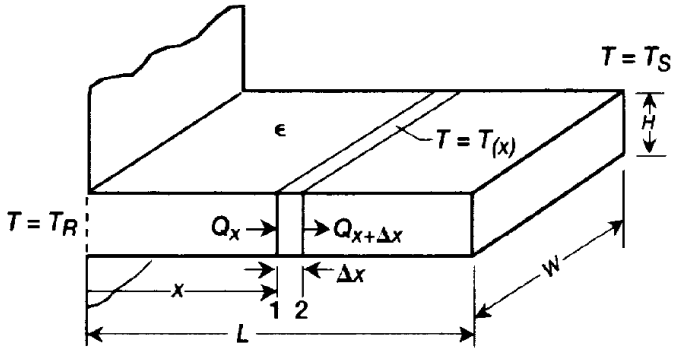

Figure 3: Parameters of 1D Radiating Fin Analysis [10].

As heat is conducted into the base of the fin, it is radiated out piecemeal until the final element radiates "all" incoming conduction ($\dot{Q}_{L-\Delta x} = \dot{Q}_{rad,L-\Delta x}$). The full temperature profile can be evaluated with the equation;

$$k_s h \frac{d^2T}{dx^2} + \sigma_{SB}\epsilon(T^4 - T_S^4) = 0 \tag{9}$$

where σ_{SB} is the Stefan-Boltzmann constant, and the boundary conditions are;

$$T(0) = T_R \tag{10}$$

$$-k_s h \frac{dT}{dx}|_L = \sigma_{SB}\epsilon(T^4 - T_S^4) \tag{11}$$

The closed form solution to this differential equation does not exist, so we take a numerical approach to iterate solutions until the boundary conditions are met with sufficient accuracy (i.e. $\dot{Q}_0 = \sum_{x=0}^{L} \dot{Q}_{rad,x}$). Finally, we can define the radiator efficiency η by comparing the total heat radiated from the fin to the "ideal" case where $T(x) = T_R$;

$$\eta = \frac{\dot{Q}_0}{LW\sigma_{SB}\epsilon(T^4 - T_S^4)} \tag{12}$$

IV RESULTS

This model has and will be used to refine the HP design for two distinct scenarios (1) benchtop testing inside a thermal vacuum chamber and (2) full scale feasibility studies. The former case is an important consideration for establishing the working principles and manufacturing limitations associated with terrestrial operation. For instance, grooved HPs are proven for many working fluids. They are simple to replicate and to visually inspect for manufacturing errors. However, when they operate in a gravitational environment there is a challenge to ensure that grooves are properly wetted at startup. An example design shown in Figure 4 could be evaluated in a thermal vacuum chamber. The capillary heat load limit is 40W compared with the 15W required to reach this operating temperature for the radiator.

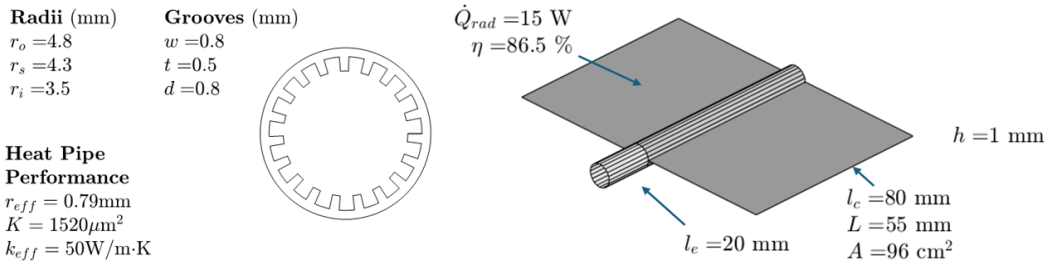

Figure 4: Wick Profile *left* and Radiator Profile *right* for an AlN HP with Ethanol. Capillary limit is 25W at 400K.

The present work focuses on the full scale case, and considers the greater question of what such a system might look like, and where is there a need for innovation or compromise. We start from the baseline established by Juhasz [10] that considered a design of a HP made from a graphite-fiber-carbon-matrix composite (or carbon-carbon, C-C). The goal is to target a 3kg/m^2 areal density and mass per unit heat rejection of <1kg/kW [3]. In Figure 5 we model an AlN HP matching the outer dimensions from the P95WG design, and internal geometry matching known groove pipe parameters.

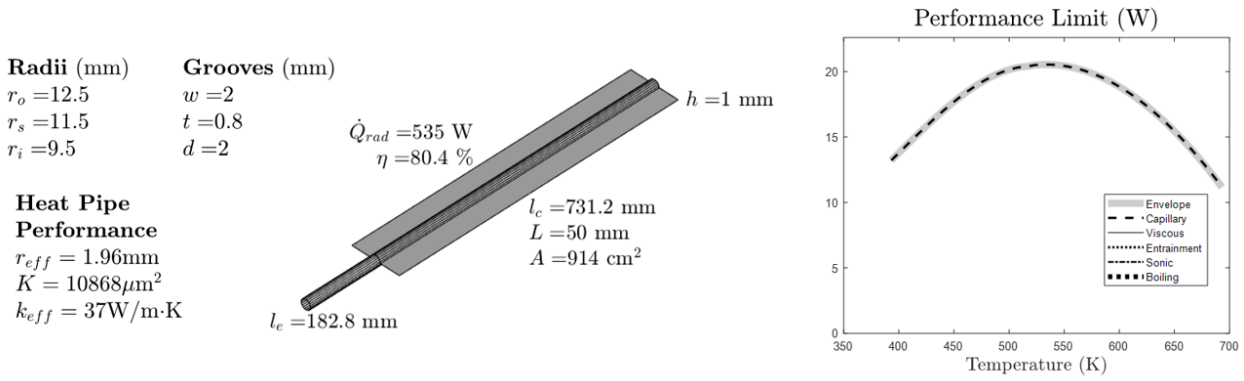

Figure 5: Reduced Order Thermal Model of Baseline AlN HP with $AlBr_3$ for Design Iteration.

The resultant areal density is 8.8 kg/m^2 and the radiative heat transfer is 535 W at

533 K, which exceeds the capillary limit 20.5 W. Strategies to improve the results include increasing the radiator length ($L\times5$), reducing the condenser length ($W/2$) and thickening the wick path to improve the permeability ($K \times 5$). Throughout, the ratio of $l_c : l_e$ was maintained at 4:1 as a means to maintain design consistency. The areal density was reduced to 5.3kg/m^2 and the capillary limit of the heat pipe increased to 177 W, but the radiator output remains infeasible at 840 W. To improve the capillary limit, the r_{eff} can be reducing. Adding a screen mesh liner on the inner profile of the groove teeth increases the capillary pressure while maintaining high permeability in the groove. Such a system is proposed by Faghri [9] and explored more thoroughly by Wong [11].

Additionally, such a feature can be additively manufactured as a lattice or similar structure, see Figure 6. The ceramic printer resolution is estimated $<50\mu$m, which is used to inform the model parameters. We estimate r_{eff} based on the wire screen mesh parameters (mesh spacing w_m, wire diameter d_m) per Table 4.

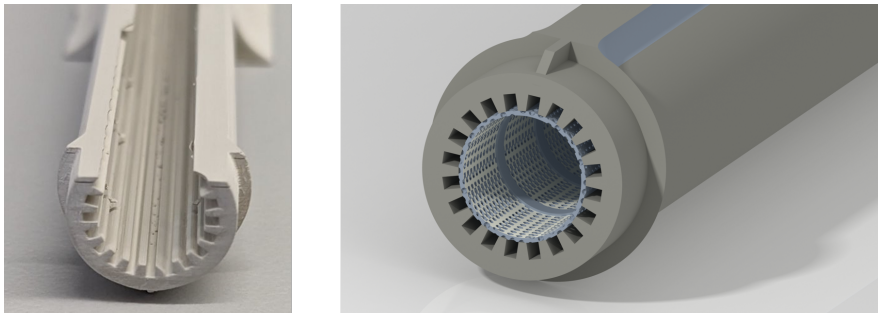

Figure 6: Printed AlN HP with Groove Wick *left* and CAD Model with Mesh Screen Style Structure *right*.

With a significant reduction in r_{eff} from 4mm $\rightarrow$ 0.05mm, the capillary limit is significantly increased and the limitation due to entrainment is mitigated completely. Design iteration permits a reduction of the mass of all components while maintaining a similar areal density (5.2kg/m^2) and vastly improved radiator efficiency (70.7%). The mass per unit of heat rejection (1.0kg/kW) is now at the target maximum of 1kg/kW. Radial heat flux at the evaporator is 4.74W/cm^2. The full design and performance is shown in Figure 7. The mass breakdown is shown in Table 5.

Table 5: Mass Breakdown in Final Radiator Design.

Component	Shell (+endcaps)	Wick	Fluid	Fin (each)	HP Subtotal	**Total**
Mass (g)	85	31	48	45	164	**254**

V SUMMARY AND CONCLUSION

A 1D reduced order model has been developed and used to establish a conceptual design of a ceramic AlN heat pipe with aluminum bromide working fluid. This work demonstrates the potential feasibility of an AlN HP to meet areal density goals for the facilitation space

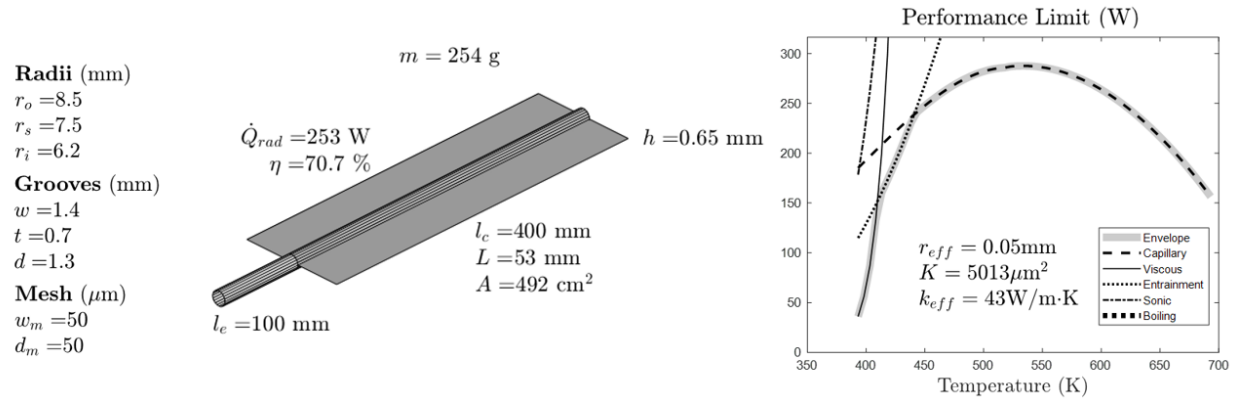

Figure 7: Final Design of AlN HP Radiator *left* and Performance Envelope *right*. This Design has Areal Density of 5.2kg/m^2, and Performance of 5.1kW/m^2, and 1.00kg/kW.

NEP systems. The final model presented has an areal density of 5.2kg/m^2, produces up to 253W of heat rejection at 1.0kg/kW, operates from 500-600K, and has a radiator efficiency of 70.7%. The wick profile is based on a combined groove and mesh screen. This design is both highly advantageous for increasing the capillary limit, and for manufacturing wick profiles with 3D printing techniques.

Future work includes developing a model of buckling, supported by experimentation, to set a baseline for wall thickness. The equation used to calculate permeability is based on metal heat pipes, so we will conduct experiments with rate-of-rise testing to scale our estimates more accurately. Additionally, the boiling limit assumes bubble nucleation occurs on smooth metal surfaces rather than ceramic printed parts, necessitating further refinement. The design of the geometry will eventually taper to blend the heat pipe and fin sections, which should lead to higher efficiencies as more of the radiating surface operates close to the fluid temperature. Lastly, remaining working fluids will be evaluated as relevant thermal properties are established.

ACKNOWLEDGEMENTS

This work is funded by NASA Early Stage Innovations grant number 80NSSC23K0236 as part of the Space Technology Research Grants program. The authors would like to thank Elaine Petro for their support with this work. The authors acknowledge the use of facilities and instrumentation supported by NSF through the Cornell University Materials Research Science and Engineering Center DMR-1719875.

References

[1] L. S. Mason, S. R. Oleson, D. T. Jacobson, P. C. Schmitz, L. Qualls, M. Smith, B. Ade, and J. Navarro, "Nuclear power concepts and development strategies for high-power electric propulsion missions to mars," 2022. [Online]. Available: www.sti.nasa.gov

[2] T. Cremins, A. K. Kludze, L. A. Dudzinski, and R. David, "Mars transportation assessment study," NASA, Tech. Rep., Mar. 2023.

[3] NASA, *Civil Space Shortfall Ranking.* Space Technology Mission Directorate, Jul. 2024. [Online]. Available: techport.nasa.gov/strategy

[4] W. S. Machemer, M. E. Duchek, and D. Nikitaev, "Considerations for Radiator Design in Multi-Megawatt Nuclear Electric Propulsion Applications," in *AIAA SCITECH 2023 Forum*, ser. AIAA SciTech Forum. American Institute of Aeronautics and Astronautics, Jan. 2023. [Online]. Available: arc.aiaa.org/doi/10.2514/6.2023-0152

[5] W. G. Anderson, C. Tarau, and D. L. Ellis, *Intermediate Temperature Heat Pipe Working Fluids*, 2018, pp. 395–423.

[6] G. D'Orazio, W. R. Sixel, and S. Sobhani, "Additive Manufacturing and Working Fluid Characterization of Ceramic Heat Pipes," in *AIAA SCITECH 2024 Forum.* Orlando, FL: American Institute of Aeronautics and Astronautics, Jan. 2024. [Online]. Available: arc.aiaa.org/doi/10.2514/6.2024-1792

[7] W. G. Anderson, R. W. Bonner, P. M. Dussinger, J. R. Hartenstine, D. B. Sarraf, I. E. Locci, and S. Louis, "Intermediate temperature fluids life tests-experiments," 2007.

[8] P. Nemec, A. Čaja, and M. Malcho, "Mathematical model for heat transfer limitations of heat pipe," *Mathematical and Computer Modelling*, vol. 57, no. 1, pp. 126–136, Jan. 2013.

[9] A. Faghri, *Heat Pipes and Thermosyphons.* Springer, 2018, pp. 2163–2211.

[10] A. J. Juhasz, "Design considerations for lightweight space radiators based on fabrication and test experience with a carbon-carbon composite prototype heat pipe," 1998.

[11] S.-C. Wong, M.-S. Deng, and M.-C. Liu, "Characterization of composite mesh-groove wick and its performance in a visualizable flat-plate heat pipe," *International Journal of Heat and Mass Transfer*, vol. 184, p. 122259, 2022. [Online]. Available: www.sciencedirect.com/science/article/pii/S0017931021013582